International Journal of Bifurcation and Chaos, Vol. 11, No. 11 (2001) 2715–2729
© World Scientific Publishing Company

CONTROL AND SYNCHRONIZATION OF SPACE EXTENDED DYNAMICAL SYSTEMS

J. BRAGARD
Center for Interdisciplinary Research on Complex Systems, Northeastern University, Boston MA 02115, USA

S. BOCCALETTI
Dept. of Phys. and Applied Math., Universidad de Navarra, Irunlarrea s/n, E-31080 Pamplona, Spain

F. T. ARECCHI
Istituto Nazionale di Ottica Applicata, Largo E. Fermi, 6, I-50125 Florence, Italy

Received October 23, 2000; Revised December 18, 2000

We discuss the issues of controlling and synchronizing continuous space extended systems in the case of two bidirectionally coupled fields, each one obeying one-dimensional CGL. When the two equations are identical, control and synchronization are achieved by means of a finite number of local tiny perturbations, selected by an adaptive technique. We address the problem of the minimum number of local perturbations needed to realize control and synchronization. When the two equations are nonidentical, we show how to induce the appearance of different kinds of synchronized states, depending on the difference in the uncoupled dynamical regimes of the considered fields. Finally, we discuss the role of space-time defects in mediating the process leading to perfect synchronization between the two systems.

1. Introduction

In the last decade, control and synchronization of temporal chaos have attracted a noticeable interest within the scientific community [Boccaletti *et al.*, 2000]. In both cases, a dynamics is conveniently disturbed, in order to force the appearance of a goal behavior $g(t)$ compatible with the natural evolution of the system. In the former case, the goal dynamics is chosen to be one of the unstable periodic orbits embedded within the chaotic attractor [Auerbach *et al.*, 1987], in the latter case it corresponds to the dynamics of another chaotic system with the aim of producing a collective dynamical evolution, which is usually called *a synchronized state.*

Since the first proposals for control [Ott *et al.*, 1990] and synchronization [Pecora & Carroll, 1990] of chaos, many other approaches have been suggested for chaos control [Pyragas, 1992; Boccaletti & Arecchi, 1995], while, the concept of synchronization has evolved to that of phase synchronization [Rosenblum *et al.*, 1996], lag synchronization [Rosenblum *et al.*, 1997], generalized synchronization [Rulkov *et al.*, 1995; Kocarev & Parlitz, 1996], intermittent lag synchronization [Rosenblum *et al.*, 1997; Boccaletti & Valladares, 2000], imperfect phase synchronization (IPS) [Zaks *et al.*, 1999], and almost synchronization (AS) [Femat & Solis-Perales, 1999]. The transition between different types of synchronization processes has been extensively studied in a pair of symmetrically coupled chaotic oscillators [Rosenblum *et al.*, 1997; Rosa *et al.*, 1998]. On the other hand, the control of chaos has been shown to be effective even in the case of delayed dynamical systems [Boccaletti *et al.*, 1997a],

by the use of the adaptive technique [Boccaletti & Arecchi, 1995].

The huge body of literature devoted to these issues is justified by the large interest that they have in practical applications, such as communicating with chaos [Hayes *et al.*, 1994], secure communication processes [Cuomo & Oppenheim, 1993; Gershenfeld & Grinstein, 1995; Kocarev & Parlitz, 1995; Peng *et al.*, 1996; Boccaletti *et al.*, 1997c], and experimental control of chaos in many areas such as e.g. chemistry [Petrov *et al.*, 1993], laser physics [Roy *et al.*, 1992; Meucci *et al.*, 1994; Meucci *et al.*, 1996], electronic circuits [Hunt, 1991], and mechanical systems [Ditto *et al.*, 1990]. Furthermore, experimental verifications of chaos synchronization have been offered e.g. in the cardiorespiratory system [Schafer *et al.*, 1998], in the human brain [Tass *et al.*, 1998], in the cells of paddlefish [Neiman *et al.*, 1999] and in communication with chaotic lasers [Van Wiggeren & Roy, 1998].

Only recently, control mechanisms have been investigated in space extended systems. After few preliminary attempts [Aranson *et al.*, 1994] to control spatiotemporal chaos, attention has been directed to the control of two-dimensional patterns [Lu *et al.*, 1996; Martin *et al.*, 1996], or of coupled map lattices [Parmananda *et al.*, 1997a; Grigoriev *et al.*, 1997], or of particular model equations, such as the Complex Ginzburg–Landau Equation [Montagne & Colet, 1997] and the Swift Hohenberg Equation for lasers [Bleich *et al.*, 1997; Hochheiser *et al.*, 1997]. Furthermore, synchronization has been proved in extended systems with unidirectional (drive-response) configuration [Parmananda, 1997b].

However, while for concentrated systems, the different proposed techniques have easily found experimental verifications, in the extended case experimental counterparts of the large body of theoretical proposals [Aranson *et al.*, 1994; Lu *et al.*, 1996; Martin *et al.*, 1996; Parmananda *et al.*, 1997a; Grigoriev *et al.*, 1997; Montagne & Colet, 1997; Bleich *et al.*, 1997; Hochheiser *et al.*, 1997; Parmananda, 1997b] are not yet available. We argue that the main reason for this lack of experiments is due to the fact that almost all proposed methods used space-extended perturbations, that is perturbations which have to be applied at any point of the system. The few examples of global control [Parmananda *et al.*, 1997a], or control with a finite number of local perturbations [Grigoriev *et al.*, 1997], were so far limited to discrete systems, i.e. to coupled map lattices. The most relevant problem in passing from concentrated to space extended continuous systems arises, indeed, when considering that an extended continuous system is an intrinsically infinite dimensional system, and it is still unclear whether the perturbation itself should be extended in space, i.e. should affect all points of the considered system. This last requirement would be, indeed, very difficult to realize experimentally, and would constitute an objective limitation for experimental implementations.

Further in this Review, we discuss how to overcome the above difficulties in the case of a bidirectional coupling between two space extended fields obeying one-dimensional CGL, for both identical (Sec. 2) and nonidentical (Sec. 3) CGL. In the former case we will show that control and synchronization can be achieved by means of a finite number of local tiny perturbations, selected by an adaptive technique and we address the problem of the minimum number of local perturbations needed to warrant the occurrence of the two processes. In the latter case, we will show that different kinds of synchronized states may be induced depending on the difference in the uncoupled dynamical regimes of the considered fields, and we will discuss the role of space-time defects in mediating the process leading to perfect synchronization between the two systems.

2. Identical Systems

2.1. *Model equation*

In this first part, we will show that both control and synchronization can be achieved in a continuous extended system by means of a *finite* number of local controllers, i.e. by a finite number of non-extended perturbations, each one affecting a different point in the system. The minimum number of controllers will be derived, and the robustness of both processes against the presence of noise will be verified.

For the sake of exemplification, we will refer to the one-dimensional Complex Ginzburg–Landau equation (CGL)

$$\dot{A} = A + (1 + i\mu_1)A_{xx} - (1 + i\mu_2)|A|^2 A\,, \qquad (1)$$

where $A(x, t) \equiv \rho(x, t)e^{i\psi(x,t)}$ is a complex field of amplitude ρ and phase ψ, dot denotes temporal derivative, A_{xx} stays for the second derivative of A

with respect to the space variable $0 \leq x \leq L$, L represents the system length, and μ_1, μ_2 are suitable real control parameters. The boundary conditions are chosen to be periodic.

Equation (1) describes the universal dynamical features of an extended system close to a Hopf bifurcation [Cross & Hohenberg, 1993], and it has been used to model many different situations in laser physics [Coullet *et al.*, 1989], fluid dynamics [Kolodner *et al.*, 1995], chemical turbulence [Kuramoto & Koga, 1981], bluff body wakes [Leweke & Provansal, 1994], etc.

Different chaotic regimes can be identified in Eq. (1) in different regions of the parameter space (μ_1, μ_2) [Shraiman *et al.*, 1992; Chate, 1994]. In particular, Eq. (1) has plane wave solutions of the type

$$A_q = \sqrt{1 - q^2} e^{i(qx + \omega t)} , \qquad (2)$$

where $-1 \leq q \leq 1$, q being the wavenumber in Fourier space, and the dispersion relation is

$$\omega = -\mu_2 - (\mu_1 - \mu_2) q^2 . \qquad (3)$$

When $\mu_1 \mu_2 > -1$, a critical value of the wavenumber $q_c = \sqrt{(1 + \mu_1 \mu_2)/(2(1 + \mu_2^2) + 1 + \mu_1 \mu_2)}$ exists, and all the plane waves in the range $-q_c \leq q \leq q_c$ are linearly stable. The plane waves outside this wavenumber range are instead unstable undergoing the so-called Eckhaus instability [Janiaud *et al.*, 1992]. As the product $\mu_1 \mu_2$ approaches -1 the critical wavenumber value vanishes, and therefore all plane waves become unstable when crossing from below the line $\mu_1 \mu_2 = -1$ in the parameter space, which is called Benjamin–Feir or Newell line. Above this line, Chate [1994] first identified three different turbulent regimes, namely phase turbulence (PT), amplitude turbulence (AT) or defect turbulence, and bichaos. In particular, we will focus our attention on PT and AT, since they have generated a special interest in the scientific community [Sakaguchi, 1990; Egolf & Greenside, 1994; Montagne *et al.*, 1996; Torcini, 1996; van Hecke, 1998].

PT is the dynamical regime characterized by a chaotic behavior of $A(x, t)$ essentially dominated by the dynamics of the phase $\psi(x, t)$, whereas the amplitude $\rho(x, t)$ changes smoothly, and it is always bounded away from zero. On the contrary, in AT the amplitude dynamics becomes dominant over the phase dynamics, and produces large amplitude oscillations which can occasionally drive $\rho(x, t)$ to zero, thus inducing the appearance of a space-time defect.

PT and AT are characterized by a spatial autocorrelation function decaying exponentially, with a spatial correlation length ξ smaller than the system size L, that is,

$$C(x, x') = \langle A(x, t) A^*(x', t) \rangle_t \simeq e^{-\frac{|x - x'|}{\xi}} , \qquad (4)$$

where $\langle \ldots \rangle_t$ denotes average in time. In two spatial dimensions it has been theoretically predicted [Coullet *et al.*, 1989] and experimentally verified [Arecchi *et al.*, 1993] that the defects have a dynamical role in mediating the shrinking process of ξ, thus in the passage from regular to turbulent behavior.

Since each domain of size ξ is space-correlated in its dynamics, the main features of the space-time chaotic evolution of the system can be captured by considering a collection of $N = \text{int}(L/\xi) + 1$ uncorrelated domains, and a single local perturbation within each domain should warrant the collapse of $A(x, t)$ onto any goal pattern $g(x, t)$ compatible with the natural evolution of the system.

In fact, we argue that the number of local perturbations necessary to slave $A(x, t)$ to a goal pattern $g(x, t)$ might be smaller than N, in virtue of nonlinear constraints within the system, which make each correlation domain interact with all the others.

In the following, we first demonstrate that the above sufficient condition holds for a judicious choice of the local perturbations, and then we will move to show that the necessary condition for the control can, in fact, be obtained with a number of local controllers smaller than N.

2.2. *Adaptive control*

Let us begin by setting $\mu_1 = 2.1$ and $\mu_2 = -1.3$ in Eq. (1) in order to enter the AT regime. In the following, we will solve numerically Eq. (1) with $L = 64$, periodic boundary conditions, and random initial conditions. The numerical code is based on a semi-implicit scheme in time with finite differences in space. The precision of the code is first order in time and second order in space. In all the simulations we use a space discretization $dx = 0.125$ (512 mesh points) and a time step for the integration $dt = 0.001$. For the above choices, the spatial correlation length is $\xi = 4.39$, corresponding roughly to 35 points of the mesh ($N = 17$). Control of

space-time chaos implies the emergence of some unstable periodic pattern out from the AT regime. Therefore, the goal pattern $g(x, t)$ is represented by any of the plane wave solutions (2), which are unstable in AT.

In order to control the system to the desired goal pattern, we add to the right-hand side of Eq. (1) a perturbative term $U(x, t)$ of the type

$$\begin{aligned} U(x, t) &= 0 \qquad \text{for } x \neq x_i \\ U(x, t) &= U_i(t) \qquad \text{for } x = x_i \end{aligned} \tag{5}$$

where $i = 1, \ldots, M$ and $x_i = 1 + (i-1)\nu$ are the positions of M local controllers, mutually separated by a distance ν ($x_{i+1} - x_i = \nu$).

As a first step of our analysis, we will use $\nu = \xi$ ($M = N$), in order to show that a sufficient condition for a robust control is that the number of controllers equals the correlation length. After that, we will show that control can be achieved also for $\nu > \xi$ ($M < N$), thus making our approach of some help for practical experimental implementations.

The strength of the M perturbations $U_i(t)$, $i = 1, \ldots, M$ is selected by the following algorithm. At each controller position x_i and integration time t_n, the ith controller measures the distance $\delta_i(t_n)$ between the actual dynamics $A(x_i, t_n)$ and the goal pattern $g(x_i, t_n)$

$$\delta_i(t_n) = A(x_i, t_n) - g(x_i, t_n)\,, \tag{6}$$

and evaluates its local variation rates

$$\lambda_i(t_n) = \log \left| \frac{\delta_i(t_n)}{\delta_i(t_{n-1})} \right|. \tag{7}$$

The perturbation is then selected as

$$U_i(t_n) = K_i(t_n)(g(x_i, t_n) - A(x_i, t_n))\,, \tag{8}$$

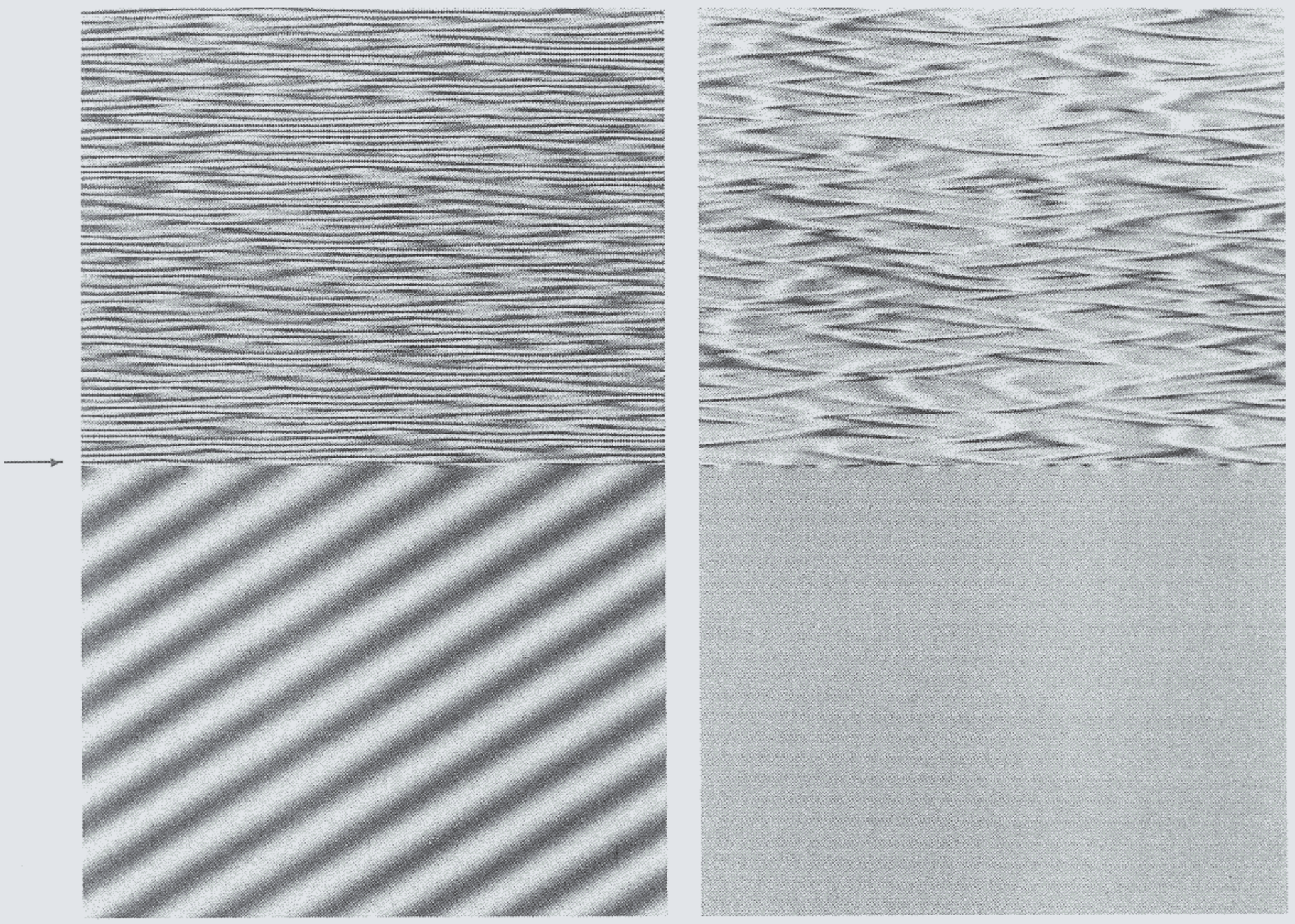

Fig. 1. Space (horizontal)-time (vertical) plots of the real part of A (left) and the modulus of A (right). Time increases downwards from 1000 to 1800 (u.t.). The first 1000 time units corresponds to the transient before the system reaches the chaotic (AT) domain starting from random initial conditions. The patterns have been coded in 256 gray levels (white corresponds to maxima). The parameters are $\mu_1 = 2.1$ and $\mu_2 = -1.3$, $dt = 0.001$, $L = 64$, $dx = 0.125$. The control ($\sigma = 0.1$, $K_0 = 1$) starts at $T = 1400$ (indicated by an arrow). The goal dynamics is chosen to be the particular plane wave solution (2) having $q = 0.589$ (corresponding to six wavelengths for this system size). The associated frequency and amplitude are $\omega = 0.12$ and $A_q = 0.808$. In these conditions, the control is reached after a very fast transient and with only $M = 17$ controllers.

where

$$\frac{1}{K_i(t_n)} = \frac{1}{K_0}(1 - \tanh(\sigma\lambda_i(t_n))),\ \sigma > 0,\ K_0 > 0. \tag{9}$$

The algorithm of Eqs. (6)–(9) is an extension of the adaptive algorithm introduced in [Boccaletti & Arecchi, 1995], and successfully applied also to chaos synchronization [Boccaletti *et al.*, 1997c], targeting of chaos [Boccaletti *et al.*, 1997b], filtering of noise from chaotic data sets [Boccaletti *et al.*, 1997d], and control of delayed dynamical systems [Boccaletti *et al.*, 1997a].

The algorithm is called *adaptive* insofar as the strength of the perturbation in Eq. (8) depends *adaptively* on the local dynamics of the system. In particular, when $A(x_i, t_n)$ naturally shadows the goal pattern $g(x_i, t_n)$, a temporal decreasing behavior of $\delta_i(t)$ is produced, which is reflected into a negative $\lambda_i(t)$ and a reduction of the weight factor $K_i(t)$ in Eq. (9). On the contrary, whenever the dynamics tends to push the system away from the goal pattern, this is reflected by a growth of $K_i(t)$. In other words, the further (closer) the system is to the goal pattern, the larger (smaller) is the weight given to the perturbation. The limit $\sigma \to 0$ of the above algorithm recovers the Pyragas' control method of [Pyragas, 1992], implying a constant weight K_0 in Eq. (9). The positive quantity σ represents the sensitivity of the method, and it plays a crucial role in assuring the smallness of the perturbations as well as the effectiveness of the control [Boccaletti & Arecchi, 1995].

Figure 1 reports the control of one of the unstable plane waves (2) for $\sigma = 0.1$ and $K_0 = 1$. The control procedure implies the suppression of the defects, until the controlled amplitude relaxes to a constant value. The arrow indicates the instant at which control is switched on.

Let us now discuss the robustness of the control against noise. For this purpose, besides the control perturbation $U(x, t)$, we add to the right-hand side of Eq. (1) a Gaussian noise $\pi(x, t)$ with

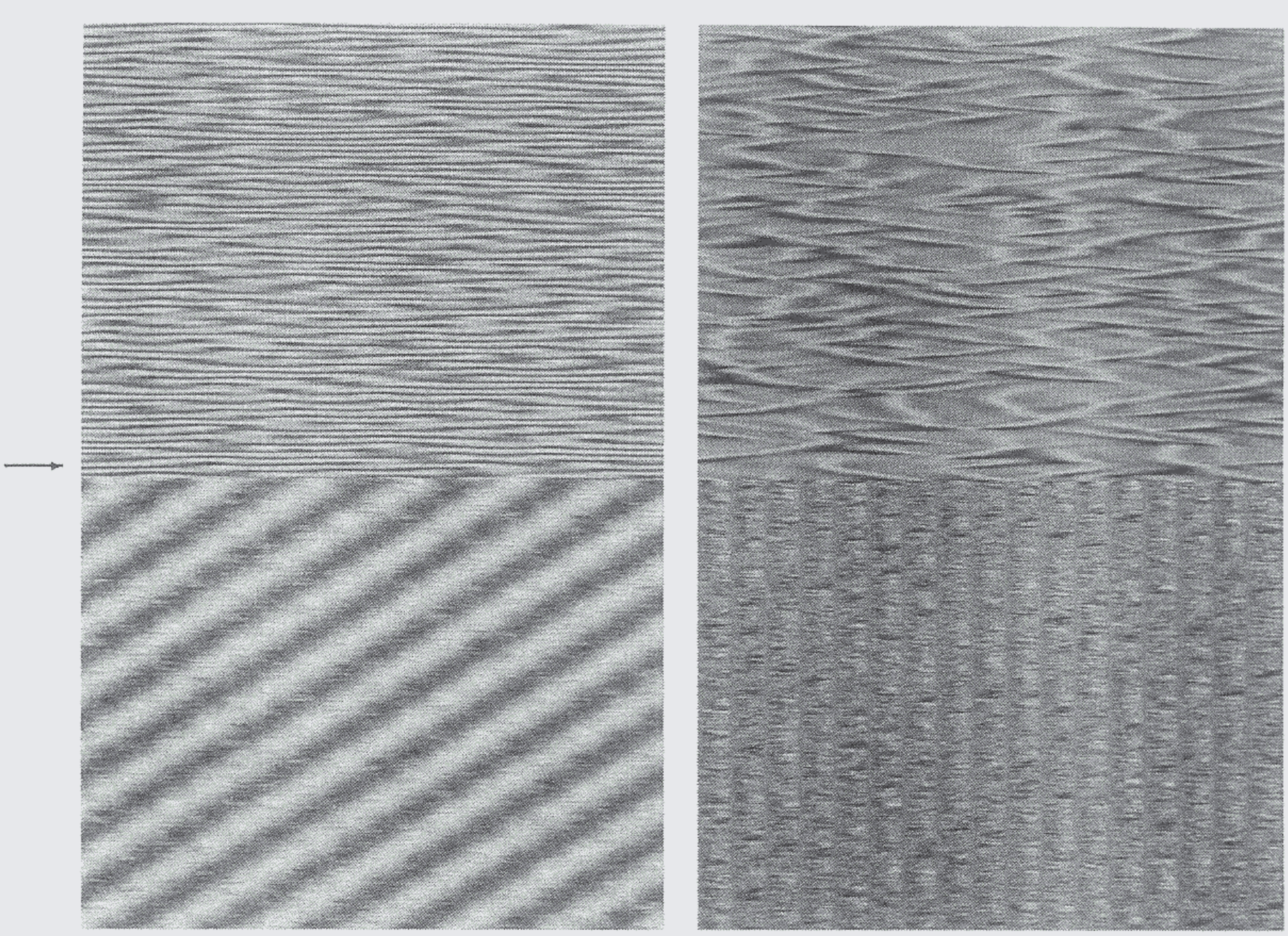

Fig. 2. Same as Fig. 1 with the addition of Gaussian noise with a standard deviation $0.01 * A_q/\sqrt{2}$ to all points of the mesh at each time step. This noise is added to both the real and imaginary parts of the field $A(x, t)$. The trace of the $M = 17$ equispaced controllers is now visible on the modulus.

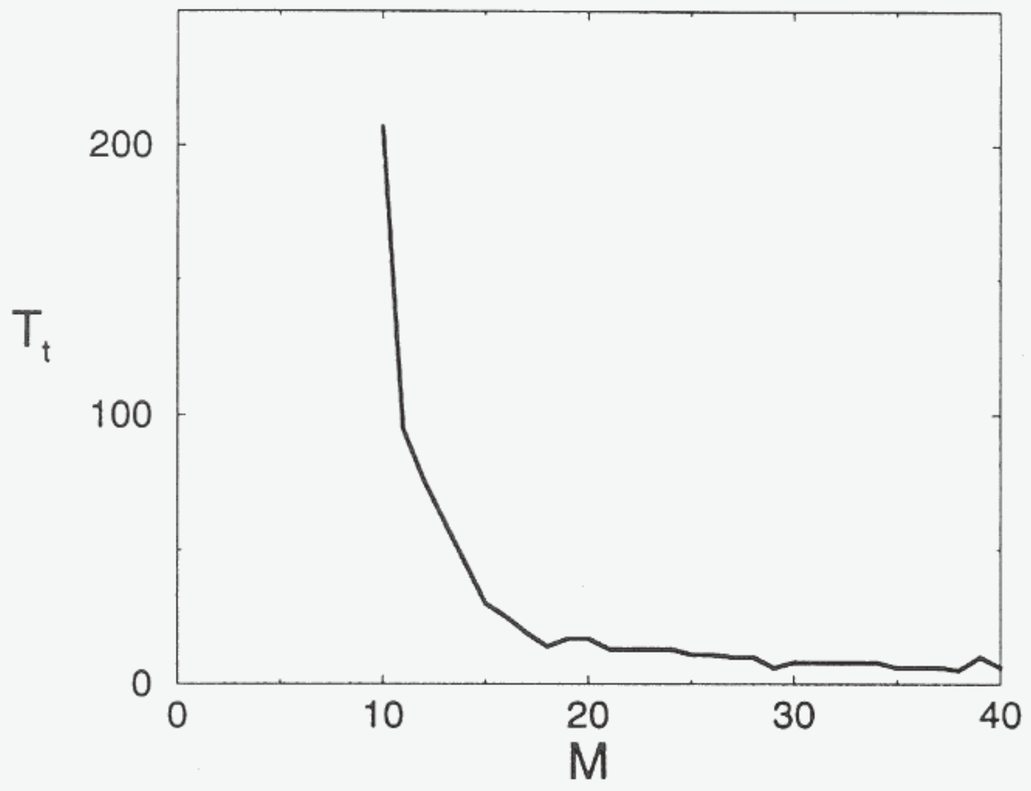

Fig. 3. Plot of the transient time T_t before achieving control as a function of the number M of equidistantly spaced controllers. Same parameters as in the caption of Fig. 1 $\mu_1 = 2.1$, $\mu_2 = -1.3$ AT regime. The proposed method fails for $M < 8$, whereas a controller with double correlation length is enough to achieve control.

zero average and delta correlated in space and time ($\langle \pi(x, t) \rangle_t = 0$ and $\langle \pi(x, t)\pi^*(x', t') \rangle = \gamma\delta(x - x')\delta(t - t')$). The results are shown in Fig. 2 for a noise strength of 1% of the unperturbed dynamics A. The control process still leads to the appearance of the desired goal pattern for relatively high noise strengths (up to 4%). The lower part of the right picture shows that noise cancelation is effective only at the controller points.

Finally, we now discuss the issue of the minimum number of requested local perturbations. Figure 3 reports the transient time T_t needed to achieve control of the plane wave of Fig. 1 versus M, showing that T_t diverges to $+\infty$ for $M < 8$. Recalling that $L = 64$ and $\xi = 4.39$, so that $N = 17$, Fig. 3 actually tells us that control is possible, unless associated with a larger transient time, even with a controller distance $\nu \simeq 2\xi$, that is with a number of controllers about one half the number of correlation domains. This improvement suggests that our adaptive method can overcome the difficulties encountered so far for experimental implementations of control of space-time chaotic states.

2.3. *Synchronization*

In this section, we discuss the problem of chaos synchronization. To this purpose, we consider two complex fields $A_1(x, t)$ and $A_2(x, t)$, each one obeying Eq. (1) with the same parameters μ_1 and μ_2 as in the above case. The two fields evolve from different random initial conditions, and therefore they produce two space and time unsynchronized AT dynamics. The algorithm of Eqs. (6)–(9) is used in order to select the perturbations at each controller point x_i, but now the goal dynamics for $A_1(x, t)$ is $A_2(x, t)$, and vice versa. In other words, the local controllers symmetrically force each complex field to collapse into the other one in particular space positions. The results are summarized in Fig. 4, for $\sigma = 0.1$ and $K_0 = 1$. The arrow indicates again the instant at which the controllers become active. The final synchronized state $A_1(x, t) = A_2(x, t)$ remains amplitude turbulent, and the process determines a complete synchronization of each space-time defect, as shown by the equality of the amplitudes A_1 and A_2.

It is important to point out that, while the proposed control process crucially relies on the knowledge of the unstable plane waves, the synchronization procedure is independent of any knowledge of the system. The local goal values for the two fields can be indeed measured by the same controllers at any time and at any controller location, thus making the synchronization process directly implementable with no need of previous knowledge on the system.

3. Nonidentical Systems

A natural question arises directly from the first part of this work: Is it possible to realize all different kinds of synchronization features in the case of a coupling between nonidentical extended systems? This problem has been only recently addressed [Boccaletti *et al.*, 1999; Chate *et al.*, 1999], and, in this second part, we summarize the main results reported by us in [Boccaletti *et al.*, 1999], presenting further analysis and a detailed discussion for the emerging synchronization states.

3.1. *The model system*

Here again, we will refer to a pair of one-dimensional fields $A_{1,2}(x, t)$, each one obeying a CGL. The system under study is

$$\dot{A}_{1,2} = A_{1,2} + (1 + i\alpha_{1,2})\partial_x^2 A_{1,2} - (1 + i\beta_{1,2})|A_{1,2}|^2 A_{1,2} + \varepsilon(A_{2,1} - A_{1,2}), \tag{10}$$

where $A_{1,2}(x, t) \equiv \rho_{1,2}(x, t)e^{(i\psi_{1,2}(x,t))}$ are two complex fields of amplitudes $\rho_{1,2}$ and phases $\psi_{1,2}$

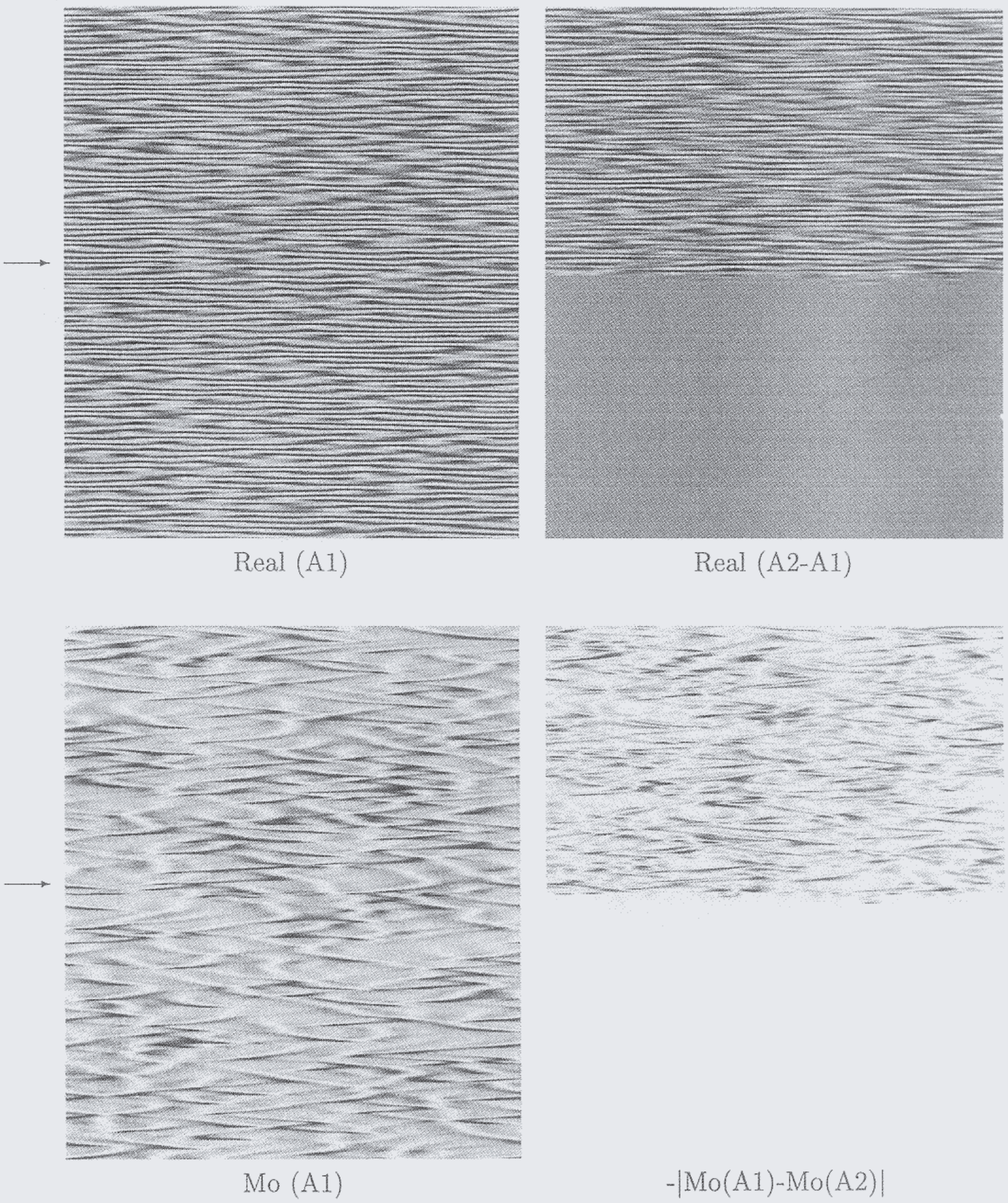

Fig. 4. Synchronization of two identical systems $A_1(x, t)$ (left column) and $A_2(x, t)$ both in the AT regime (same parameters as in Fig. 1). The right columns display the differences between the two patterns (upper: real parts, lower: moduli). The time runs from 1000 to 1600 (u.t) and the synchronization starts at $T = 1300$ (indicated by an arrow).

respectively, $\alpha_{1,2}$, $\beta_{1,2}$ are suitable real parameters, and ε is the strength of the symmetric coupling.

It is important to remark that we deal here with nonidentical systems ($\alpha_1 \neq \alpha_2$, $\beta_1 \neq \beta_2$), so that two different cases must be taken into account, namely the small and large parameter mismatch cases. For small parameter mismatches, the systems are prepared in the same dynamical regime, e.g. both in PT or in AT. On the contrary, for large parameter mismatches, α_1, α_2, β_1, β_2 are chosen so as one system is in the PT regime, while the other is in the AT regime.

3.2. *AT–AT case*

Let us first consider the case of small parameter mismatches, and select $\alpha_1 = \alpha_2 = 2.1$, $\beta_1 = -1.25$, $\beta_2 = -1.2$ in Eq. (10) (both fields in AT). Figure 5

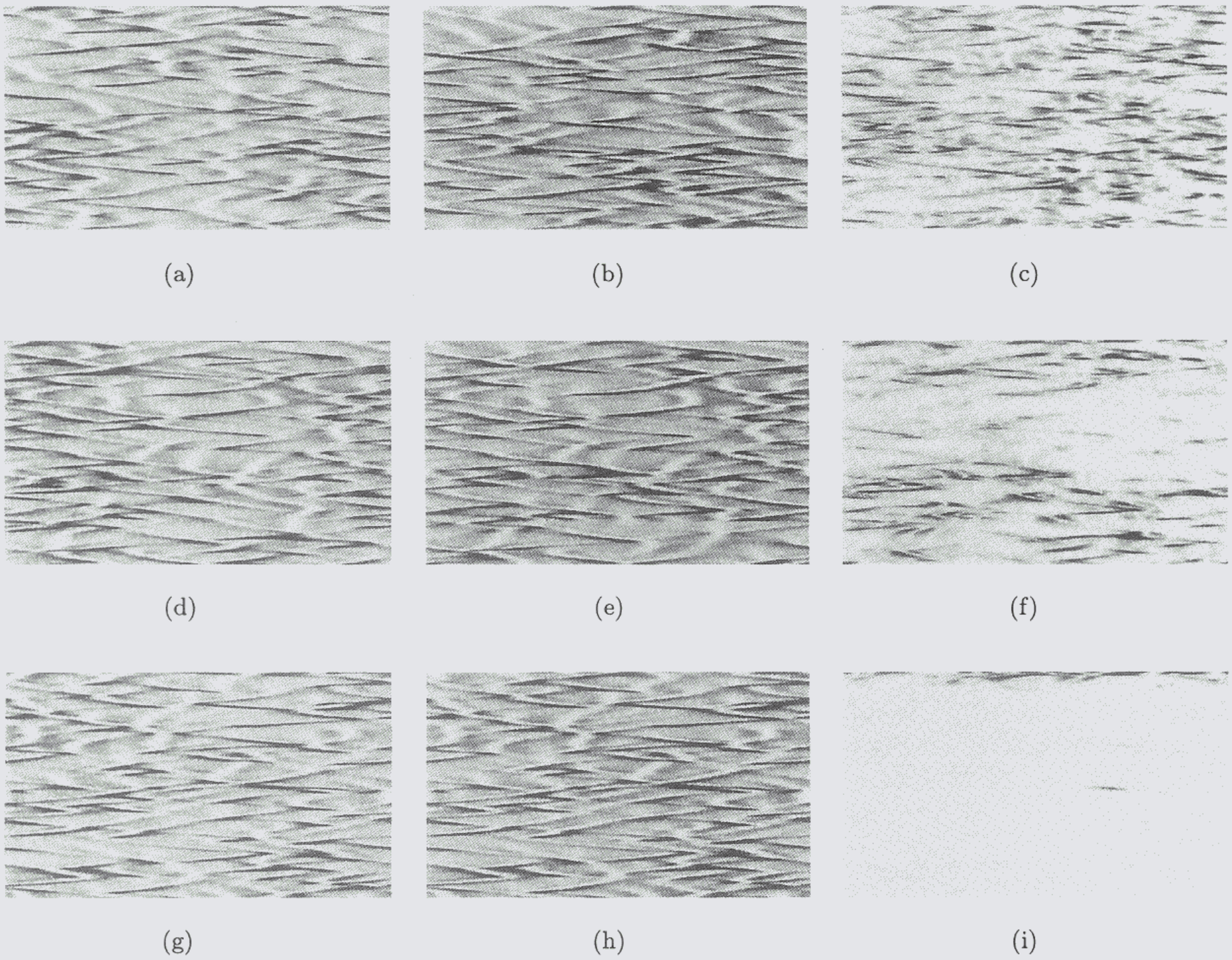

Fig. 5. *AT–AT Case:* Space (horizontal)-time (vertical) plots of (a, d, g) ρ_1, (b, e, h) ρ_2 and (c, f, i) $-|\rho_1 - \rho_2|$. $\alpha_1 = \alpha_2 = 2.1$, $\beta_1 = -1.25$, $\beta_2 = -1.2$. Time increases downwards from 300 to 600 (u.t.). The first 300 time units (not plotted) corresponds to the transient before the system reaches two independent chaotic (AT) states starting from two independent random initial conditions; (a, b, c) correspond to $\varepsilon = 0.05$, (d, e, f) to $\varepsilon = 0.09$, (g, h, i) to $\varepsilon = 0.15$. In (c, f, i) the white regions correspond to $|\rho_1 - \rho_2| = 0$, i.e. indicate complete synchronization.

reports the space-time plots of ρ_1 [Figs. 5(a), 5(d), 5(g)], ρ_2 [Figs. 5(b), 5(e), 5(h)] $|\rho_1 - \rho_2|$ [Figs. 5(c), 5(f), 5(i)] for $\varepsilon = 0.05$ [Figs. 5(a)–5(c)], $\varepsilon = 0.09$ [Figs. 5(d)–5(f)] and $\varepsilon = 0.15$ [Figs. 5(g)–5(i)]. In all cases, the patterns come out from a codification into a 256 gray levels scale and the dark lines in [Figs. 5(a), 5(b), 5(d), 5(e), 5(g), 5(h)] trace the positions of the space-time defects. The simulations of Eq. (10) have been performed with $L = 64$, periodic boundary conditions and random initial conditions.

From Fig. 5 one can infer the existence of a gradual passage from a nonsynchronized AT state [Figs. 5(a)–5(c) to a completely synchronized AT state [Figs. 5(g)–5(i)], through an intermediate state [Figs. 5(d)–5(f)] wherein partial synchronization is built.

At variance with what happens in concentrated systems, here the transition from nonsynchronized to synchronized states is not associated with the presence of an intermediate PS regime. Indeed, Fig. 6 reports the measurements of $\langle \Delta\rho \rangle = \langle |\rho_1 - \rho_2| \rangle$ and $\langle \Delta\psi \rangle = \langle |\psi_1 - \psi_2| \rangle$ versus ε ($\langle \ldots \rangle$ stays for an averaging in both time and space), and shows that $\langle \Delta\rho \rangle(\varepsilon)$ and $\langle \Delta\psi \rangle(\varepsilon)$ gradually decay at once. The scenario is therefore consistent with what has been already observed for small parameter mismatches in chemical models [Parmananda, 1997b].

3.3. *PT–PT case*

The above scenario does not change qualitatively when we consider a coupling between two initial PT states. Let us choose $\alpha_1 = \alpha_2 = 2.1$, $\beta_1 = -0.75$, $\beta_2 = -0.83$ in Eq. (10) (both fields in PT), and, by gradually increasing ε, perform simulations with the same system size, boundary conditions and initial

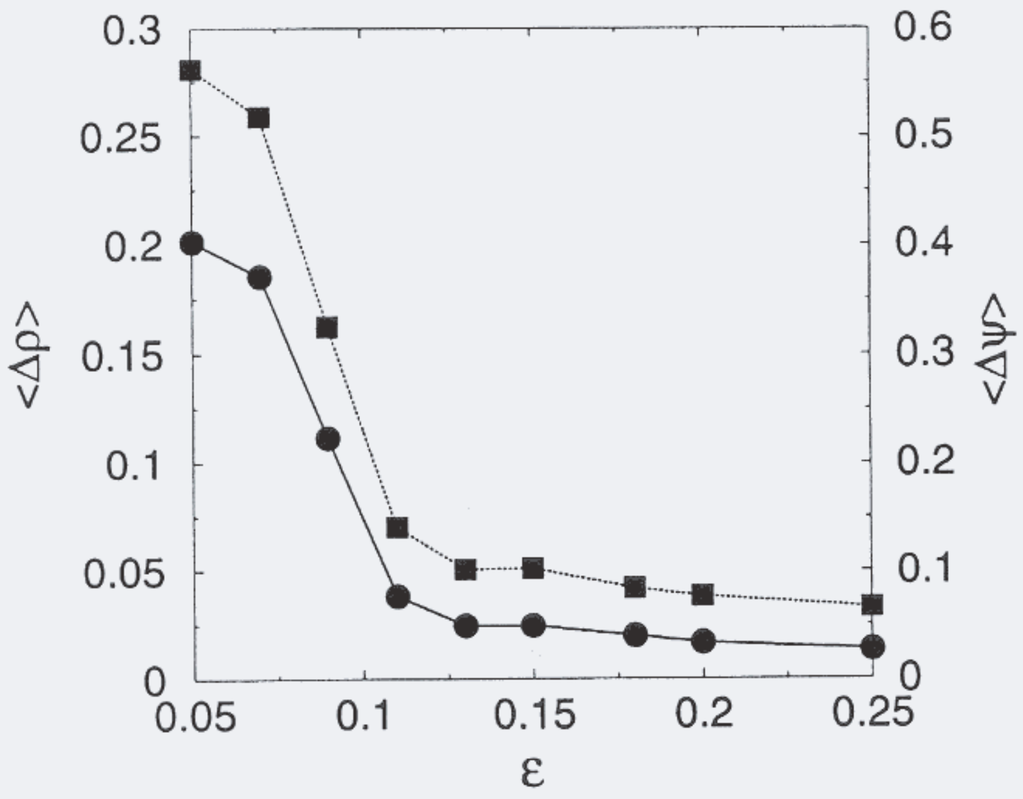

Fig. 6. *AT–AT Case:* Indicators of modulus (•) and phase (■) synchronization. Space-time average of the difference between amplitudes and phases of the two fields versus the coupling ε (see definitions in the text). Same parameters as in the caption of Fig. 5. The left (right) vertical axis reports the $\langle\Delta\rho\rangle(\langle\Delta\psi\rangle)$ scale.

conditions as above. The results are shown in Fig. 7, where we report ρ_1 [Figs. 7(a), 7(d)], ρ_2 [Figs. 7(b), 7(e)] $|\rho_1 - \rho_2|$ [Figs. 7(c), 7(f)] for two values of the coupling parameter $\varepsilon = 0.02$ [Figs. 7(a)–7(c)] and $\varepsilon = 0.04$ [Figs. 7(d)–7(f)]. Here again, the system passes from an unsynchronized PT state at small couplings to a completely synchronized PT state. In this case, since defects are not present the synchronization emerges for a smaller coupling strength.

3.4. *Large parameter mismatch*

A much richer scenario is observed in the case of large parameter mismatches. Let us select in Eq. (10) $\alpha_1 = \alpha_2 = 2.1$, $\beta_1 = -1.2$, $\beta_2 = -0.83$. This implies that the field A_1 is evolving in AT, while the field A_2 is evolving in PT. In Fig. 8 we report the patterns arising from the space-time representations of ρ_1 [Figs. 8(a), 8(d), 8(g)], ρ_2 [Figs. 8(b), 8(e), 8(h)] $|\rho_1 - \rho_2|$ [Figs. 8(c), 8(f), 8(i)] for $\varepsilon = 0.03$ [Figs. 8(a)–8(c)], $\varepsilon = 0.14$ [Figs. 8(d)–8(f)] and $\varepsilon = 0.19$ [Figs. 8(g)–8(i)].

At small coupling strengths, the two systems do not synchronize, and they hold in their respective regimes [Figs. 8(a)–8(c)]. At large coupling strengths, the two systems reach a CS regime, which is realized in PT [Figs. 8(g)–8(i)]. The final synchronized state is space-time chaotic, but the synchronization process is associated with the suppression of all defects, which were initially present in A_1.

However, the most interesting regime is the intermediate one [Figs. 8(d)–8(f)], with the two systems giving rise to a partial synchronization phenomenon realized in an AT regime.

In Fig. 9 we report the plots of $\langle\Delta\rho\rangle$ and $\langle\Delta\psi\rangle$ versus ε. In contrast with Fig. 6, Fig. 9 highlights

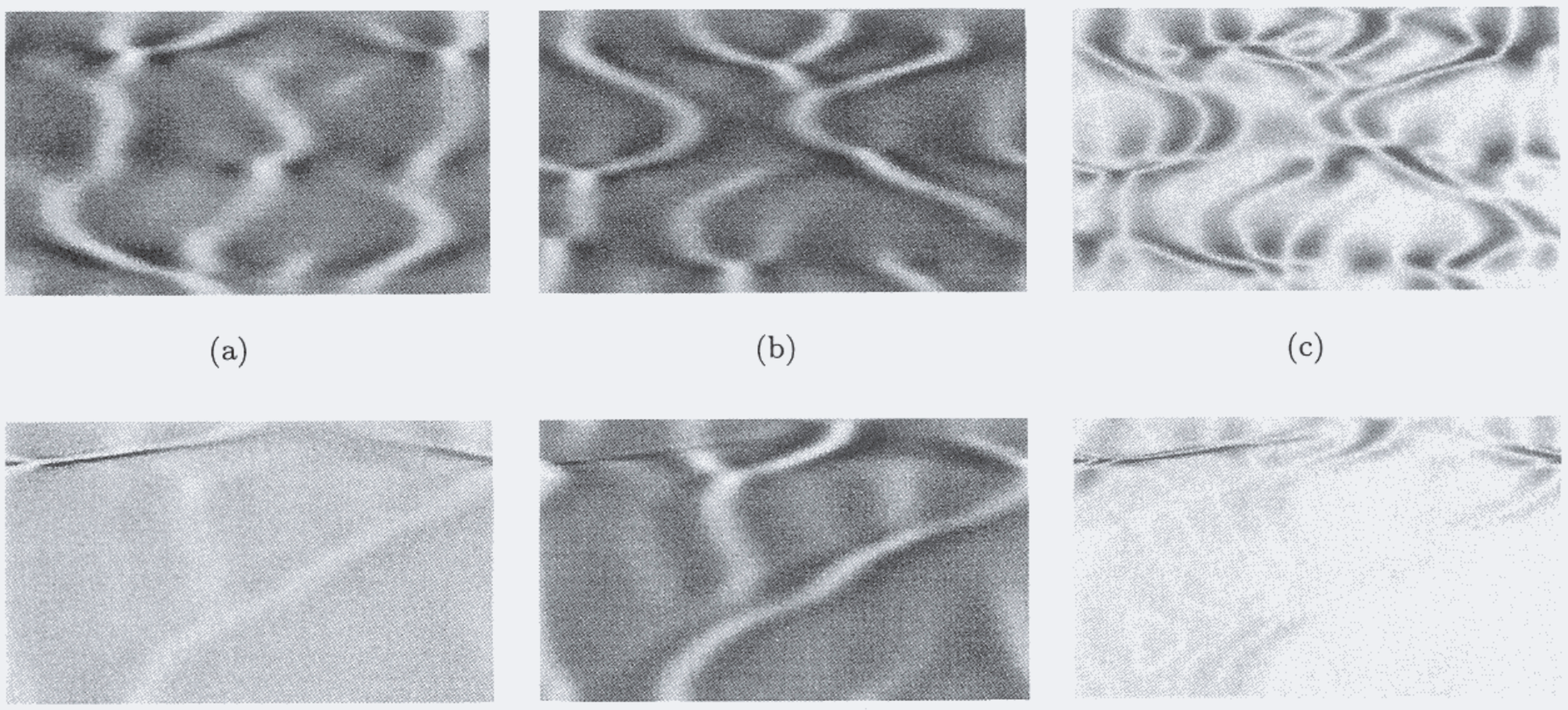

Fig. 7. *PT–PT Case:* Space (horizontal)-time (vertical) plots of (a, d) ρ_1, (b, e) ρ_2, and (c, f) $-|\rho_1 - \rho_2|$. $\alpha_1 = \alpha_2 = 2.1$, $\beta_1 = -0.75$, $\beta_2 = -0.83$. Other parameters, initial conditions and boundary conditions as in Fig. 5. Same stipulations as in Fig. 5; (a–c) correspond to $\varepsilon = 0.02$, (d–f) to $\varepsilon = 0.04$.

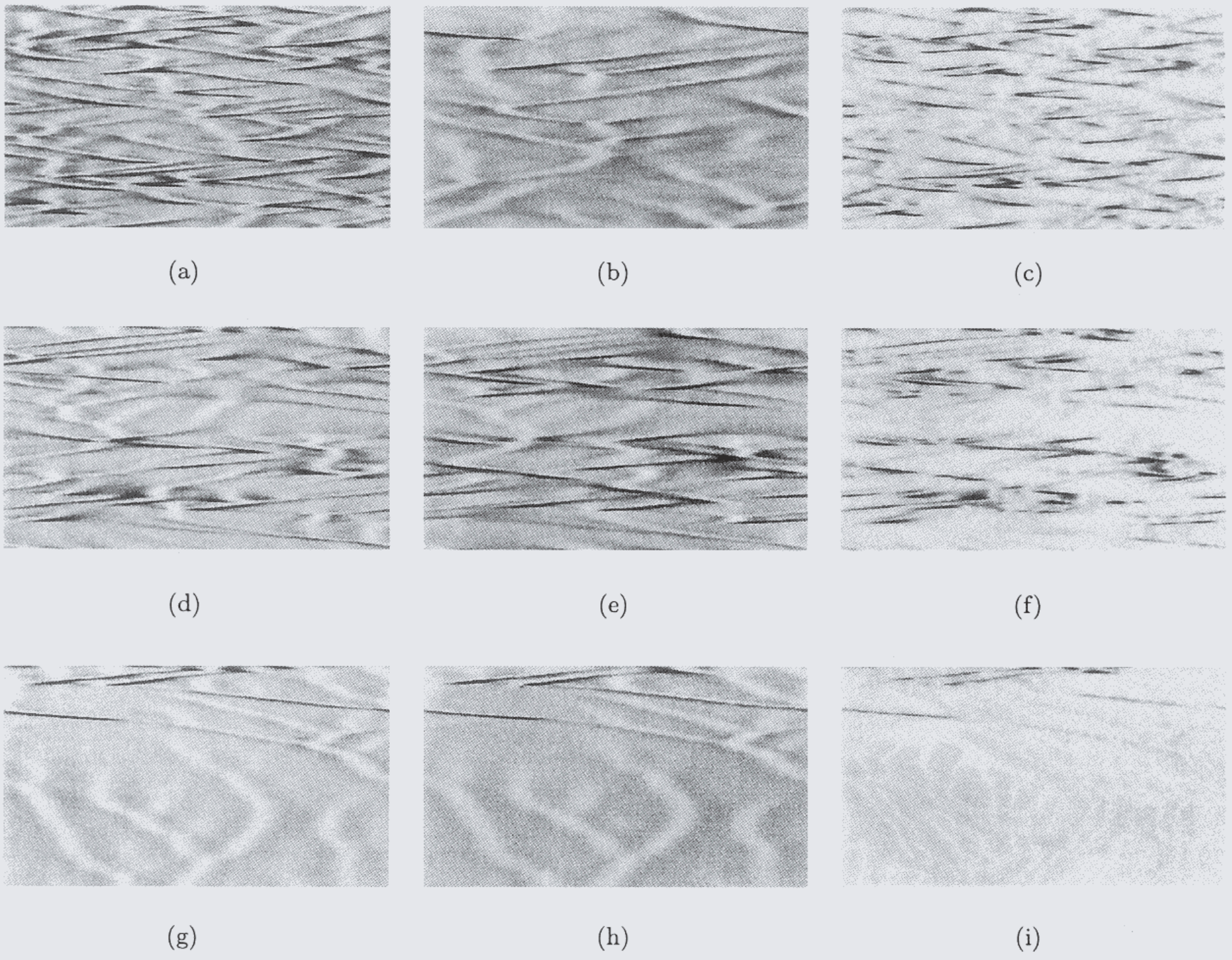

Fig. 8. *AT–PT Case:* Space (horizontal)-time (vertical) plots of (a, d, g) ρ_1, (b, e, h) ρ_2, and (c, f, i) $-|\rho_1 - \rho_2|$. $\alpha_1 = \alpha_2 = 2.1$, $\beta_1 = -1.2$, $\beta_2 = -0.83$. Other parameters, initial conditions and boundary conditions as in Figs. 5 and 7. Same stipulations as in Figs. 5 and 7; (a–c) correspond to $\varepsilon = 0.03$, (d–f) to $\varepsilon = 0.14$, (g–i) to $\varepsilon = 0.19$.

the presence of a wide range of ε ($0.1 \leq \varepsilon \leq 0.16$) for which amplitude synchronization is not yet reached [see Fig. 8(f)], but the average phase distance converges to a constant value. In this situation, one expects the amplitudes of the two fields to be uncorrelated, while the phases already strongly coupled.

An heuristic argument for such a phenomenon can be offered. The natural evolution of A_1 is in AT, that is showing the presence of many space-time defects. Defects are localized points wherein the amplitude of the field vanishes. As a consequence, in each one of them, the phase ψ_1 shows a singularity. AT allows flexibility in the amplitude dynamics, but the variations of the phase are not flexible, since they are substantially determined by the local amplitude variations. On the contrary, A_2 would naturally evolve in PT, that is with a dominant phase dynamics. The phase ψ_2 is not naturally bounded, and its oscillations are allowed by the evolution of the uncoupled systems. For $0.1 \leq \varepsilon \leq 0.16$, a strong correlation is built in the phases. There, ψ_1 and ψ_2 converge in average (apart from a constant). This is possible only when ψ_2 locally adjusts on ψ_1. The relevant consequence of this process is the introduction of many defects in the field A_2, which would be instead free of them in the uncoupled state.

As a conclusion of this part, we can state that, while for small parameter mismatches one observes a passage from no synchronized to completely synchronized states, for large parameter mismatches this transition is mediated by a state which is similar to what was called phase synchronization for concentrated systems. In the former case, the resulting space-time synchronized state is not qualitatively different from the unsynchronized one, in the latter case, the state of the system resulting from the synchronization process may substantially

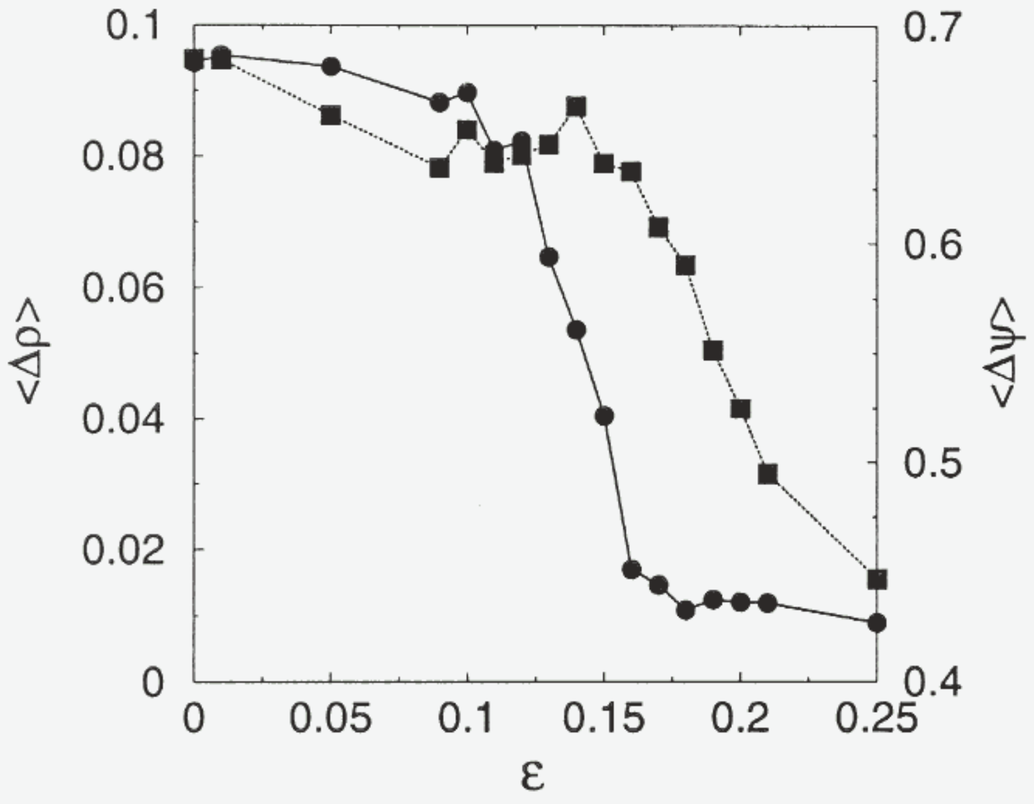

Fig. 9. *AT–PT Case:* Indicators of modulus (•) and phase (■) synchronization (same stipulations as in Fig. 6). Parameters, initial and boundary conditions as in the caption of Fig. 8. Note the phase plateau for $0.1 \leq \varepsilon \leq 0.16$.

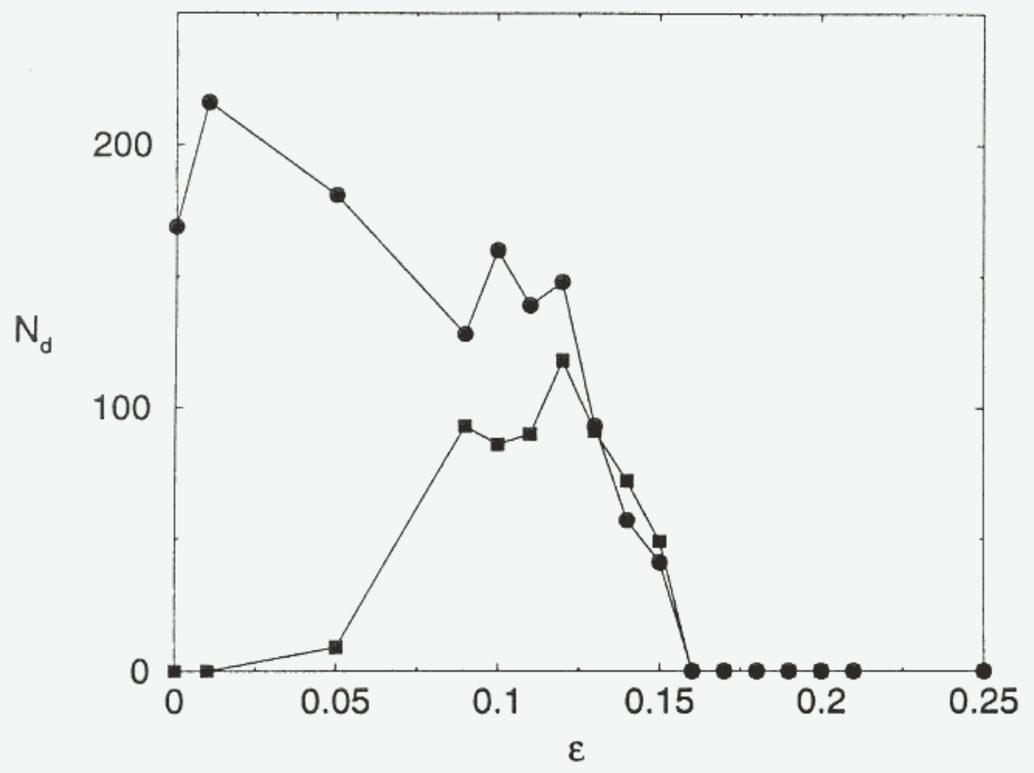

Fig. 10. *AT–PT Case:* Total number of phase defects N_d as a function of the coupling strength ε for A_1 (•) and A_2 (■). Same parameters, initial and boundary conditions as in the caption of Fig. 8.

differ from that present with no coupling, and it is mainly dictated by the synchronization process of the space-time defects. The presence of phase synchronization in CGL has been recently offered also in the case of a unidirectional coupling [Junge & Parlitz, 2000].

3.5. *Quantitative indicators for synchronization*

Now we move to the issue of quantitatively confirming the above qualitative picture for the large parameter mismatch case. For this purpose we measure the total number of phase defects N_d as a function of ε for $\alpha_1 = \alpha_2 = 2.1$, $\beta_1 = -1.2$, $\beta_2 = -0.83$. Figure 10 reports N_d versus ε for A_1 (•) and A_2 (■). At small coupling strengths ($0 < \varepsilon < 0.1$) the two fields evolve in an unsynchronized manner. At intermediate ε values ($0.1 < \varepsilon < 0.16$) it appears evident a process of defect injection into the field A_2 up to the point ($\varepsilon \simeq 0.16$) where both fields show the same defect number. Finally, when all defects have been synchronized, the system begins to reach a CS state, which is realized in PT, implying the absence of phase defects in both fields (as it is evident from Fig. 10).

The above indicator is a global indicator, that is an average on both space and time. In order to distinguish whether this synchronization phenomenon is a temporal phenomenon, a spatial phenomenon or a spatiotemporal phenomenon, we have to analyze separately the space and time features of the synchronized pattern. This can be done by moving to the Fourier space ($x \to k, t \to \Omega$) and considering $\tilde{A}_{1,2}(k, \Omega)$, that is the Fourier transforms of the fields $A_{1,2}(x, t)$. For each ε value, let us consider the following mean quantities

$$\begin{aligned} \langle k \rangle_{1,2}(\varepsilon) &\equiv \frac{1}{N_{1,2}} \int_{-k_m}^{+k_m} \int_{-\Omega_m}^{+\Omega_m} \\ &\quad \times k |\tilde{A}_{1,2}(k, \Omega)|^2 \mathrm{d}k\mathrm{d}\Omega \,, \\ \langle \Omega \rangle_{1,2}(\varepsilon) &\equiv \frac{1}{N_{1,2}} \int_{-k_m}^{+k_m} \int_{-\Omega_m}^{+\Omega_m} \\ &\quad \times \Omega |\tilde{A}_{1,2}(k, \Omega)|^2 \mathrm{d}k\mathrm{d}\Omega \,, \end{aligned} \tag{11}$$

where $\Omega_m \equiv (N\pi)/(t_t)$, $k_m \equiv (N\pi)(L)$, N is the total number of discrete data considered for the Fourier transform, t_t is the total running time of the simulation, and the normalization constants $N_{1,2}$ are defined by

$$N_{1,2} \equiv \int_{-k_m}^{+k_m} \int_{-\Omega_m}^{+\Omega_m} |\tilde{A}_{1,2}(k, \Omega)|^2 \mathrm{d}k\mathrm{d}\Omega \,. \tag{12}$$

Notice that both Ω_m and k_m depend on the particular discretization used in the simulations. The results show that $\langle k \rangle_{1,2}(\varepsilon) \simeq 0$ independently on ε, as one should have expected considering the fact that turbulent regimes in the CGL come out from large wavelength instabilities. On the contrary, the quantities $\langle \Omega \rangle_{1,2}$ are always bounded away from zero and strongly depend on the coupling strength. Figure 11

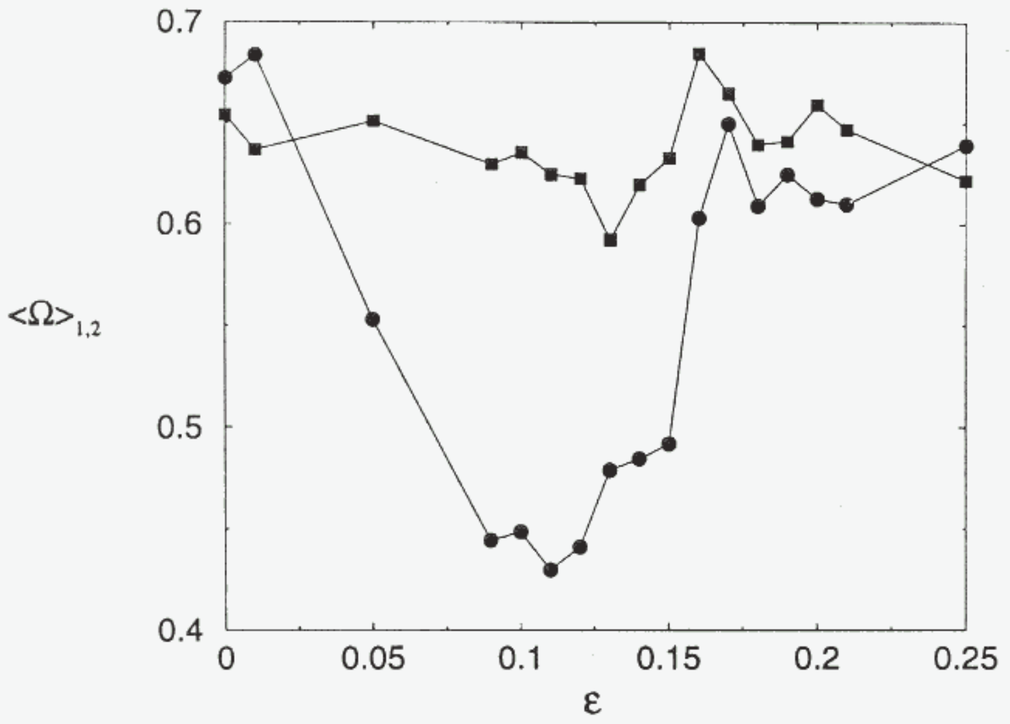

Fig. 11. *AT–PT Case:* $\langle\Omega\rangle_1$ (■) and $\langle\Omega\rangle_2$ (•) as functions of ε (see text for definitions). $\alpha_1 = \alpha_2 = 2.1$, $\beta_1 = -1.2$, $\beta_2 = -0.83$. Other parameters, initial and boundary conditions as in the caption of Fig. 8.

reports $\langle\Omega\rangle_1$ (■) and $\langle\Omega\rangle_2$ (•) as a function of ε for $\alpha_1 = \alpha_2 = 2.1$, $\beta_1 = -1.2$, $\beta_2 = -0.83$. While the field A_1 appears to be robust in the variation of its temporal frequency, the field A_2 shows a large variation in its frequency as a function of the coupling, thus confirming our heuristic argument about the flexibility of A_2 during the synchronization process.

This suggests to consider for $|\rho_1 - \rho_2|$ and $|\psi_1 - \psi_2|$ only spatial averages, as opposed to what we have considered in Figs. 6 and 9 and to investigate the temporal evolution of such new averaged differences at different ε values.

Let us then define $\langle|\rho_1 - \rho_2|\rangle_x(t)$, $\langle|\psi_1 - \psi_2|\rangle_x(t)$ the spatial averages of the differences in amplitudes and phases of the two fields (now $\langle\ldots\rangle_x$ indicates an averaging only along the spatial variable x). In

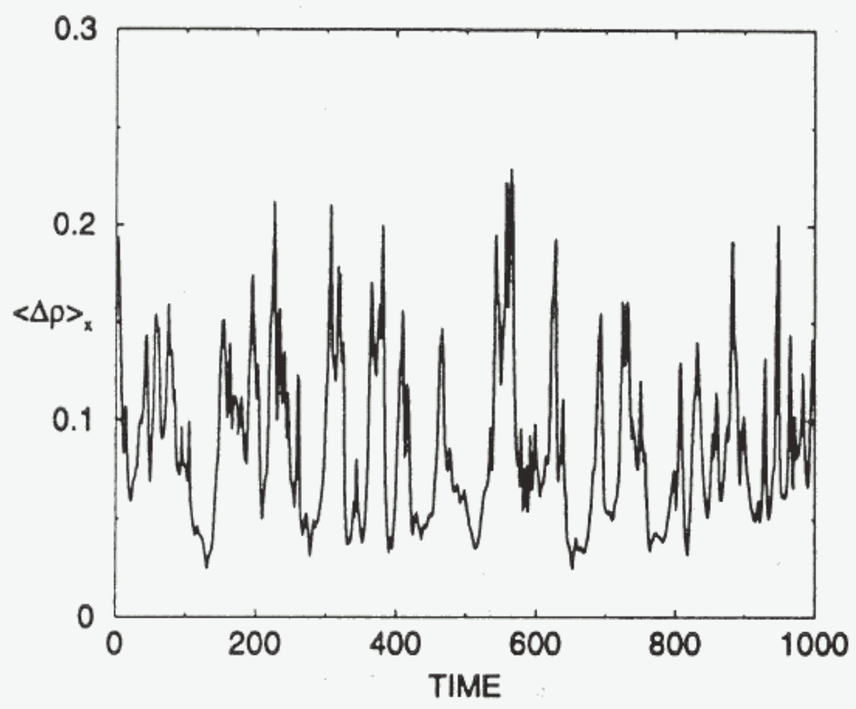

(a)

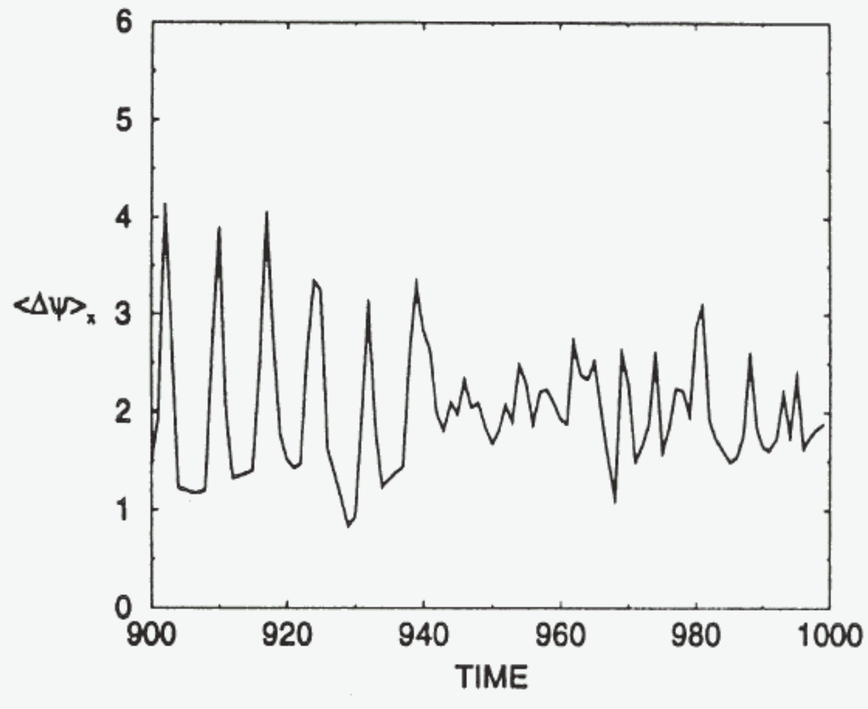

(b)

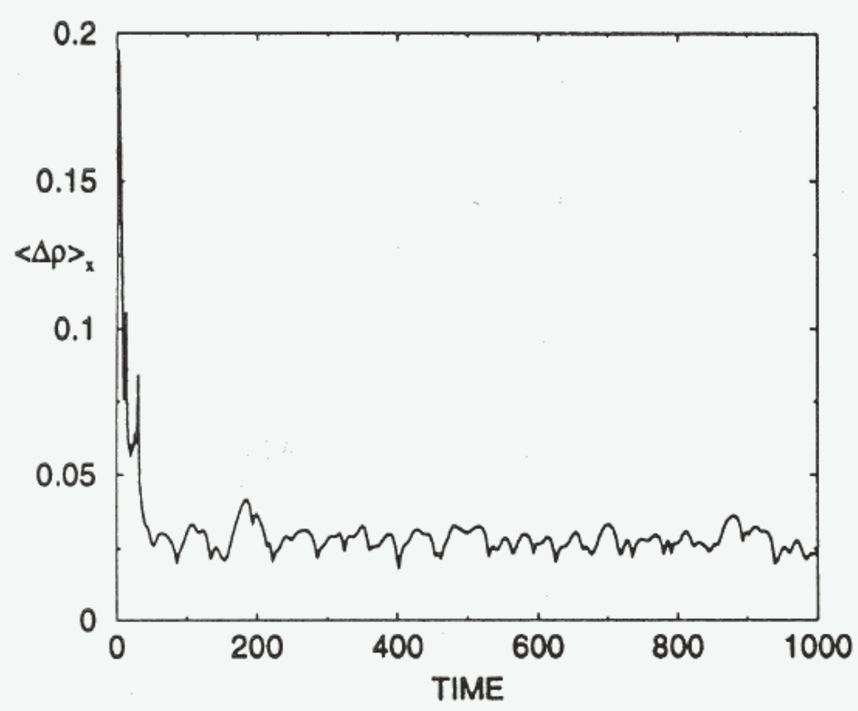

(c)

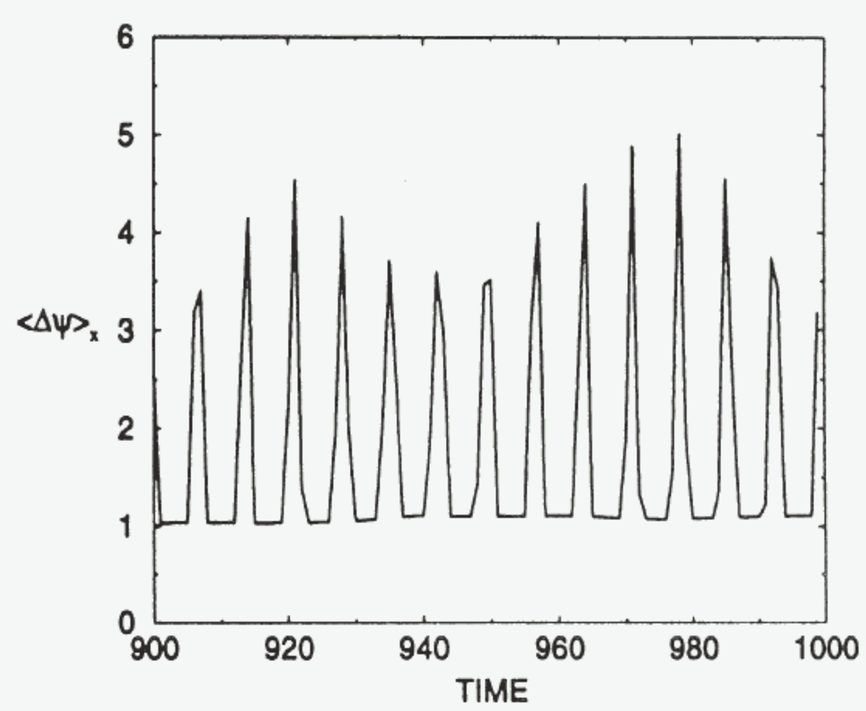

(d)

Fig. 12. *AT–PT Case:* $\langle|\rho_1 - \rho_2|\rangle_x$ (a, c) and $\langle|\psi_1 - \psi_2|\rangle_x$ (b, d) versus time (see text for definitions) for (a, b) $\varepsilon = 0.14$ and (c, d) $\varepsilon = 0.17$. $\alpha_1 = \alpha_2 = 2.1$, $\beta_1 = -1.2$, $\beta_2 = -0.83$. Other parameters, initial and boundary conditions as in the caption of Fig. 8.

Fig. 12 we show how $\langle|\rho_1 - \rho_2|\rangle_x(t)$ [Figs. 12(a), 12(c)] and $\langle|\psi_1 - \psi_2|\rangle_x(t)$ [Figs. 12(b), 12(d)] evolve in time for $\varepsilon = 0.14$ [Figs. 12(a), 12(b)] and $\varepsilon = 0.17$ [Figs. 12(c), 12(d)], that is immediately before and after the point $\varepsilon \simeq 0.16$ for which both fields show the same defect number N_d (see Fig. 10). The transition to a completely synchronized state (occurring for $\varepsilon > 0.16$) corresponds to the appearance of a regular periodic behavior for the spatial average of the difference in phase. Correspondingly, the fluctuations of $\langle|\rho_1 - \rho_2|\rangle_x(t)$ are strongly washed out. It is important to remark that, while Fig. 12 depicts the behavior of the system close to the transition, from Fig. 9 one can appreciate that the spatiotemporal average $\langle\Delta\psi\rangle$ further decreases for increasing $\varepsilon > 0.17$. Therefore, a question arises on how the temporal behavior of $\langle|\psi_1 - \psi_2|\rangle_x(t)$ accomodates with the decreasing process of $\langle\Delta\psi\rangle$, and on whether the amplitude fluctuations of $\langle|\psi_1 - \psi_2|\rangle_x(t)$ decrease, eventually vanishing at very large ε values.

4. Discussion and Conclusions

We have discussed the emergence of synchronization features in a pair of coupled nonidentical spatially extended pattern forming systems, with reference to the one-dimensional Ginzburg–Landau Equation, that is referring to a general case of an extended system undergoing an Hopf bifurcation. We have distinguished three main cases, namely identical systems, systems with a small parameter mismatch and systems with a large parameter mismatch.

For identical systems, control and synchronization can be achieved by means of a limited number of local controllers, whose distance in space may overcome the spatial autocorrelation length.

For systems displaying small parameter mismatches, the coupling induces a gradual transition toward a completely synchronized state, which is realized in the same dynamical regime recovered by the uncoupled systems.

Finally, for systems displaying large parameter mismatches, high coupling strengths induce a complete synchronized state, which is realized in phase turbulence, while intermediate coupling strengths realize partial synchronization features. The introduction of suitable indicators for analyzing space and time effects highlights that the transition between the two above synchronization states is associated with the emergence of a periodic temporal behavior for the space average on the phase difference.

Acknowledgments

The authors would like to acknowledge J. Kurths, H. L. Mancini and A. Pikovski for helpful discussions, and W. González-Viñas for the help with the imaging software. Work was partly supported by Integrated Action Italy-Spain HI97-30. S. Boccaletti acknowledges financial support from EU Contract n. ERBFMBICT983466.

References

Aranson, I., Levine, H. & Tsimring, L. [1994] "Controlling spatio-temporal chaos," *Phys. Rev. Lett.* **72**, 2561–2564.

Arecchi, F. T., Boccaletti, S., Ramazza, P. L. & Residori, S. [1993] "Transition from boundary to bulk controlled regimes in optical pattern formation," *Phys. Rev. Lett.* **70**, 2277–2280.

Auerbach, D., Cvitanovic, P., Eckmann, J.-P., Gunaratne, G. & Procaccia, I. [1987] "Exploring chaotic motion through periodic orbits," *Phys. Rev. Lett.* **58**, 2387–2389.

Bleich, M. E., Hochheiser, D., Moloney, J. V. & Socolar, E. S. [1997] "Controlling extended systems with spatially filtered, time-delayed feedback," *Phys. Rev.* **E55**, 2119–2126.

Boccaletti, S. & Arecchi, F. T. [1995] "Adaptive control of chaos," *Europhys. Lett.* **31**, 127–132.

Boccaletti, S., Maza, D., Mancini, H., Genesio, R. & Arecchi, F. T. [1997a] "Control of defects and space-like structures in delayed dynamical systems," *Phys. Rev. Lett.* **79**, 5246–5249.

Boccaletti, S., Farini, A., Kostelich, E. J. & Arecchi, F. T. [1997b] "Adaptive targeting of chaos," *Phys. Rev.* **E55**, R4845–R4848.

Boccaletti, S., Farini, A. & Arecchi, F. T. [1997c] "Adaptive synchronization of chaos for secure communication," *Phys. Rev.* **E55**, 4979–4981.

Boccaletti, S., Giaquinta, A. & Arecchi, F. T. [1997d] "Adaptive recognition and filtering of noise using wavelets," *Phys. Rev.* **E55**, 5393–5397.

Boccaletti, S., Bragard, J., Arecchi, F. T. & Mancini, H. L. [1999] "Synchronization in non-identical extended systems," *Phys. Rev. Lett.* **83**, 536–539.

Boccaletti, S., Grebogi, C., Lai, Y. C., Mancini, H. & Maza, D. [2000] "The control of chaos: Theory and applications," *Phys. Rep.* **329**, 103–197.

Boccaletti, S. & Valladares, D. L. [2000] "Characterization of intermittent lag synchronization," *Phys. Rev.* **E62**, 7497–7500.

Chaté, H. [1994] "Spatiotemporal intermittency regimes of the one-dimensional complex Ginzburg–Landau equation," *Nonlinearity* **7**, 185–204.

Chaté, H., Pikovsky, A. & Rudzick, O. [1999] "Forcing oscillatory media: Phase kinks vs. synchronization," *Physica (Amsterdam)* **D113**, 17–30.

Coullet, P., Gil, L. & Roca, F. [1989] "Optical vortices," *Opt. Commun.* **73**, 403–408.

Cross, M. & Hohenberg, P. C. [1993] "Pattern formation out of equilibrium," *Rev. Mod. Phys.* **65**, 851–1112.

Cuomo, K. M. & Oppenheim, A. V. [1993] "Circuit implementation of synchronized chaos with applications to communications," *Phys. Rev. Lett.* **71**, 65–68.

Ditto, W. L., Rauseo, S. N. & Spano, M. L. [1990] "Experimental control of chaos," *Phys. Rev. Lett.* **65**, 3211–3214.

Egolf, D. & Greenside, H. [1994] "Relation between fractal dimension and spatial correlation length for extensive chaos," *Nature (London)* **369**, 129–131.

Femat, R. & Solis-Perales, G. [1999] "On the chaos synchronization phenomena," *Phys. Lett.* **A262**, 50–60.

Gershenfeld, N. & Grinstein, G. [1995] "Entrainment and communication with dissipative pseudorandom dynamics," *Phys. Rev. Lett.* **74**, 5024–5027.

Grigoriev, R. O., Cross, M. C. & Schuster, H. G. [1997] "Pinning control of spatiotemporal chaos," *Phys. Rev. Lett.* **79**, 2795–2798.

Hayes, S., Grebogi, C., Ott, E. & Mark, A. [1994] "Experimental control of chaos for communication," *Phys. Rev. Lett.* **73**, 1781–1784.

Hochheiser, D., Moloney, J. V. & Lega, J. [1997] "Controlling optical turbulence," *Phys. Rev.* **A55**, R4011–R4014.

Hunt, E. R. [1991] "Stabilizing high-period orbits in a chaotic system: The diode resonators," *Phys. Rev. Lett.* **67**, 1953–1955.

Janiaud, B., Pumir, A., Bensimon, D., Croquette, V., Richter, H. & Kramer, L. [1992] "The Eckaus instability for travelling waves," *Physica (Amsterdam)* **D55**, 269–286.

Junge, L. & Parlitz, U. [2000] "Phase synchronization of coupled Ginzburg–Landau equations," *Phys. Rev.* **E62**, 438–441.

Kocarev, L. & Parlitz, U. [1995] "General approach for chaotic synchronization with applications to communications," *Phys. Rev. Lett.* **74**, 5028–5031.

Kocarev, L. & Parlitz, U. [1996] "Generalized synchronization, predictability and equivalence of unidirectionally coupled dynamical systems," *Phys. Rev. Lett.* **76**, 1816–1819.

Kolodner, P., Slimani, S., Aubry, N. & Lima, R. [1995] "Characterization of dispersive chaos and related states of binary fluid convection," *Physica (Amsterdam)* **D85**, 165–224.

Kuramoto, Y. & Koga, S. [1981] "Turbulized rotating chemical waves," *Prog. Theor. Phys. Suppl.* **66**, 1081–1085.

Leweke, T. & Provansal, M. [1994] "Model for the transition in bluff body wakes," *Phys. Rev. Lett.* **72**, 3174–3177.

Lu, W., Yu, D. & Harrison, R. G. [1996] "Control of patterns in spatiotemporal chaos in optics," *Phys. Rev. Lett.* **76**, 3316–3319.

Martin, R., Scroggie, A. J., Oppo, G.-L. & Firth, W. J. [1996] "Stabilization, selection and tracking of unstable patterns by Fourier space techniques," *Phys. Rev. Lett.* **77**, 4007–4010.

Meucci, R., Gadomski, W., Ciofini, M. & Arecchi, F. T. [1994] "Experimental control of chaos by means of weak parametric perturbations," *Phys. Rev.* **E49**, R2528–R2531.

Meucci, R., Ciofini, M. & Abbate, R. [1996] "Suppressing chaos in lasers by negative feedback," *Phys. Rev.* **E53**, R5537–R5540.

Montagne, R., Hernández-García, E. & San Miguel, M. [1996] "Winding number instability in the phase-turbulence regime of the complex Ginzburg–Landau equation," *Phys. Rev. Lett.* **77**, 267–270.

Montagne, R. & Colet, P. [1997] "Nonlinear diffusion control of spatiotemporal chaos in the complex Ginzburg–Landau equation," *Phys. Rev.* **E56**, 4017–4024.

Neiman, A., Pei, X., Russell, D., Wojtenek, W., Wilkens, L., Moss, F., Braun, H. A., Huber, M. T. & Voigt, K. [1999] "Synchronization of the noisy electrosensitive cells in the paddlefish," *Phys. Rev. Lett.* **82**, 660–663.

Ott, E., Grebogi, C. & Yorke, J. A. [1990] "Controlling chaos," *Phys. Rev. Lett.* **64**, 1196–1199.

Parmananda, P., Hildebrand, M. & Eiswirth, M. [1997a] "Controlling turbulence in coupled map lattice systems using feedback techniques," *Phys. Rev.* **E56**, 239–244.

Parmananda, P. [1997b] "Generalized synchronization of spatiotemporal chemical chaos," *Phys. Rev.* **E56**, 1595–1598.

Pecora, L. M. & Carroll, T. L. [1990] "Synchronization in chaotic systems," *Phys. Rev. Lett.* **64**, 821–824.

Peng, J. H., Ding, E. J., Ding, M. & Yang, W. [1996] "Synchronizing hyperchaos with a scalar transmitted signal," *Phys. Rev. Lett.* **76**, 904–907.

Petrov, V., Gaspar, V., Masere, J. & Showalter, K. [1993] "Controlling chaos in the Belousov–Zhabotinsky reaction," *Nature* **361**, 240–243.

Pyragas, K. [1992] "Continuous control of chaos by self-controlling feedback," *Phys. Lett.* **A170**, 421–428.

Rosa, E., Jr., Ott, E. & Hess, M. H. [1998] "Transition to phase synchronization of chaos," *Phys. Rev. Lett.* **80**, 1642–1645.

Rosenblum, M. G., Pikovsky, A. S. & Kurths, J. [1996] "Phase synchronization of chaotic oscillators," *Phys. Rev. Lett.* **76**, 1804–1807.

Rosenblum, M. G., Pikovsky, A. S. & Kurths, J. [1997] "From phase to lag synchronization in coupled chaotic oscillators," *Phys. Rev. Lett.* **78**, 4193–4196.

Roy, R., Murphy, T. W., Jr., Maier, T. D., Gills, Z. & Hunt, E. R. [1992] "Dynamical control of chaotic laser: Experimental stabilization of a globally coupled system," *Phys. Rev. Lett.* **68**, 1259–1262.

Rulkov, N. F., Sushchik, M. M., Tsimring, L. S. & Abarbanel, H. D. I. [1995] "Generalized synchronization of chaos in directionally coupled chaotic systems," *Phys. Rev.* **E51**, 980–994.

Sakaguchi, H. [1990] "Breakdown of the phase dynamics," *Prog. Theor. Phys.* **84**, 792–800.

Schafer, C., Rosemblum, M. G., Kurths, J. & Abel, H. H. [1998] "Heartbeat synchronized with ventilation," *Nature* **392**, 239–240.

Shraiman, B., Pumir, A., van Saarloos, W., Hohenberg, P. C., Chate, H. & Holen, M. [1992] "Spatiotemporal chaos in the one-dimensional complex Ginzburg–Landau equation," *Physica (Amsterdam)* **D57**, 241–248.

Tass, P., Rosenblum, M. G., Weule, M. G., Kurths, J., Pikovsky, A., Volkmann, J., Schnitzler, A. & Freund, H. J. [1998] "Detection of $n : m$ phase locking from noisy data: Application to magnetoencephalography," *Phys. Rev. Lett.* **81**, 3291–3294.

Torcini, A. [1996] "Order parameter for the transition from phase to amplitude turbulence," *Phys. Rev. Lett.* **77**, 1047–1050.

van Hecke, M. [1998] "Building blocks of spatiotemporal intermittency," *Phys. Rev. Lett.* **80**, 1896–1899.

Van Wiggeren, G. D. & Roy, R. [1998] "Communication with chaotic lasers," *Science* **279**, 1198–1200.

Zaks, M. A., Park, E.-H., Rosenblum, M. G. & Kurths, J. [1999] "Alternating locking ratios in imperfect phase synchronization," *Phys. Rev. Lett.* **82**, 4228–4231.